Computational Modeling on Mitochondrial Channel Nanotoxicity

Michael González-Durruthy[a,b*], Amal Kanta Giri[a,c,d*], Irina Moreira[c], Riccardo Concu[a], André Melo[a], Juan M. Ruso[b], M. Natália D. S. Cordeiro[a, *]

[a]*LAQV@REQUINTE-Department of Chemistry and Biochemistry, Faculty of Science, University of Porto, 4169-007 Porto, Portugal.*
[b]*Soft Matter and Molecular Biophysics Group, Department of Applied Physics, University of Santiago de Compostela, 15782 Santiago de Compostela, Spain.*
[c]*Center for Neuroscience and Cell Biology, University of Coimbra, 3004-517 Coimbra, Portugal*
[d]*Helmholtz Institute Erlangen-Nürnberg for Renewable Energy, Forschungszentrum Jülich, Fürther Straße 248, 90429 Nürnberg, Germany*

***To whom correspondence should be addressed**:
M. González-Durruthy, Email: michael.durruthy@fc.up.pt, Fax: +351220402659.
A. K. Giri, Email: amal.giri@fc.up.pt, Fax: +351220402659.
M. Natália D. S. Cordeiro, Email: ncordeir@fc.up.pt, Fax: +351220402659

Abstract

Herein, we evaluated the interactions between the zig-zag-single-walled carbon nanotube (z-z-SWCNT (8.0)) and the ATP-entry-point of the human mitochondrial voltage-dependent anion-selective channel (hVDAC1). For this purpose, both molecular docking and molecular dynamics simulations were performed. The flexibility of the referred ATP-entry-point was efficiently modeled, using the information gathered from the respective Ramachandran plot. The preferred conformations for this segment, obtained with this procedure, we were able to establish very favorable interactions with the ligands (ATP and z-z-SWCNT). Next, using both molecular docking and molecular dynamics simulations, we demonstrated that z-z-SWCNT can directly prevent the ATP-transition from its first entry-point residue (MET1). We suggested that the associated z-z-SWCNT aggregation can be responsible by avoiding the natural biochemical steps for the ATP-transport, according to a nanotoxicity mechanism based on hydrophobic interactions. The docking free energy of z-z-SWCNT/hVDAC1 and ATP/hVDAC1 complexes was remarkably close, according to local perturbation maps of the catalytic residues' cluster (*i.e.* MET1, ARG2, GLY3, SER4, ALA5). On the other hand, the results of molecular dynamics simulations match the ones of the docking simulations, reinforcing the hVDAC1 channel nanotoxicity hypothesis. Overall, the obtained results open new opportunities towards the rational design of new carbon nanomaterials and *in silico* mitotarget drug-discovery.

Introduction

The human mitochondrial voltage-dependent anion-selective channel (hVDAC1) is the main communication route between the mitochondrial inter-membrane space and cytosol.[1-3] From a structural point of view, the hVDAC1 channel is the most densely localized protein in the outer mitochondrial membrane of all human cells, which shows a β-barrel architecture composed by 19 β-strands with the N-terminal-(α)-helix segment located horizontally midway within the pore.[4-5] This segment adopts different conformations in the voltage-gating channel, depending on the external and/or internal stimuli. In all the eukaryotic cells, the biochemical functions of this segment include for example the bioenergetic regulation, membrane potential generation, the metabolic control cross-talk between the mitochondrial matrix and cytosol, the sucrose exchange, the intracellular [Ca^{2+}] regulation, the (Mg^{2+}, Zn^{+}, Na^{+}, K^{+}, etc.) ions transport, the regulation of glycolysis by association with hexokinase and the ADP/ATP-influx/efflux in hVDAC1.[5-6] In this regard, several pathological conditions-like: cancer diseases, Alzheimer, Parkinson's disease, epilepsy, acute cardiac ischemia and, many others chronic processes have been associated with different degrees of hVDAC1-channel physiological perturbations leading to mitochondrial dysfunction by loss of regulation of the mitochondrial volume and promoting apoptosis.[5-7] Three specific regions, within the N-terminal-(α)-helix segment, are directly involved in the ATP-transport and efflux. These are the ATP-entry point composed by the residue cluster (MET1, ARG2, GLY3, SER4, ALA5), the ATP-catalytic-point (ARG18) and the ATP-exit-point (LYS35). The most representative effect in the hVDAC1 channel dysfunction is the redox and bioenergetic imbalance, due to perturbations in the ATP-transport from the ATP-entry-point in the facing-inward conformation in mitochondrial matrix to the ATP-exit-point with facing outward conformation to the cytosol.[1, 8-10]

Nowadays, nanobiotechnology has brought a significant impact for ~~to~~ many fields of modern science especially with the development of novel nanomaterials like carbon nanotubes.[11] Despite these materials have having been used for a wide range of biomedical applications; they have been also associated with many hazardous effects.[12-15] This stresses the importance to develop appropriate methodologies (*in silico* tools), ~~for~~ to predict and minimize the risk associated with those applications towards safe use.[12] The potential mitochondrial nanotoxicity (*i.e.,* bioenergetics dysfunction or mitotoxic effects) induced by single-walled carbon nanotubes (SWCNT), has ~~have~~ been especially studied in the last 5 years due to their potential biomedical applications in mitochondrial nanomedicine for cancer therapy (*i.e.,* SWCNT inducing cytotoxicity-based mitochondrial bioenergetics dysfunction).[12-15] Besides, through applying new nanoinformatics concepts on mitotarget modeling and drug-discovery of highly selective carbon nanomaterials with optimal structural nanodescritors, low off-target effects and good risk/benefit relationships.

Currently, several scientific reports highlight that SWCNT can induce potential mitochondrial channel nanotoxicity on critical human mitochondrial adenine-nucleotide transport channels like the ADP/ATP carrier and hVDAC1 channels.[12-15] According to this, previous computational-experimental studies on Nano-Quantitative Structure-Binding Relationships (QSBR) models[12-13] have suggested the existence of a singular correlation between the zig-zag geometry of the z-z-SWCNT (Hamada index $m = 0$, $n > 0$) with greater mitochondrial nanotoxicity-based reactivity compared with their non-zig-zag geometric counterparts like amchair-SWCNT (Hamada index $m = n$) and chiral-SWCNT (Hamada index $m \neq n$ and $m > 0$).[12-13] However, until the present, the mechanisms involved in the mitochondrial channel nanotoxicity-inducing ATP-bioenergetic dysfunction of carbon nanotubes remain largely ignored; and some computational methodologies could provide further insights on this subject. In particular, molecular docking and molecular dynamics (MD) simulations could be very useful frameworks for addressing these issues at an atomistic level.[12-18]

One of the main challenges, associated with these approaches, is the extremely high dimensionality of the ligand-protein conformational space. Particularly, the elastic normal mode with anisotropic network (ENM-ANM models) have been widely applied for describing the protein conformational dynamic, post-translational modifications, communication properties and signal propagation in the residue network of proteins under unperturbed (*i.e.,* native conformation in the absence of ligands) and/or perturbed conditions like induced by some ~~a~~ given ligands (including nanoparticles).[19-22]

Herein, we suggest that the ENM-ANM approaches could be efficiently applied to capture the local-perturbations in the inter-residue network forming the ATP-entry-point of the N-terminal-(α)-helix segment of hVDAC1 channel, in the absence or presence of ligands (z-z-SWCNT and/or ATP the native hVDAC1-substrate).[22]

Herein, the main objective of this work is to investigate the ability of a zig-zag-single-walled carbon nanotubes (by simplicity referred as z-z-SWCNT (8.0) ligand-model) to induce mitochondrial channel nanotoxicity by selectively blocking the ATP-entry-point in hVDAC1, and disturbing the signal communication efficiency within its catalytic residue cluster (MET1, ARG2, GLY3, SER4, and ALA5). According to this, the immediate relevance of the modeling data could impact on: i) development of fast screening methods on potential human mitochondrial nanotoxicity using "human proteins" (*i.e.,* hVDAC1 crystallographic .pdb models) long before clinical studies in human candidates, in accordance with ethical criteria in nanotoxicology, ii) efficient identification of therapeutically relevant channel-binding sites for mitochondrial nanomedicine, iii) rational optimization of structural determinants (nanodescriptors) of the channel mitotoxicity, and iv) improve the *in silico* methods on 3Rs principles (reduction, refinement and replacement) of animal testing in nanotoxicology research.

To probe the ~~such~~ hypothesis, the critical interactions between the ligands (ATP native-substrate and z-z-SWCNT) and the ATP-entry-point of the hVDAC1 channel were evaluated. For this purpose, we used molecular docking, ENM-ANM analysis and molecular dynamics (MD) simulations.[12-18]

Finally, the present work gives a significant contribution to substantially improve ~~substantially~~ the rational-design of new and safe carbon nanotubes. Opening new opportunities for promising mitochondrial nanomedicine, and making regulatory decisions in nanotoxicology.

Materials and methods

Theoretical Characterization of the Zig-Zag Single Walled Carbon Nanotube

For modeling and characterizing the electronic structure of the z-z-SWCNT crystal specie ~~was used~~ the small crystal approach based on the reciprocal zone-folding (ZF) method with Wannier orthogonal functions was used. [23-25] These latter functions can be expressed as follows:

$$\emptyset_{R-SWCNT}(r) = \frac{1}{\sqrt{N}}\sum_k e^{-ik\cdot R}\psi_k(r)\ ) \quad \textbf{(1)}$$

where the Wannier functions, $\psi_k(r)$ represent the periodicity of z-z-SWCNT (8.0) ligand-model and are defined as:

$$\psi_k(r) = e^{ik\cdot r}u_k(r) \qquad \textbf{(2)}$$

In these equations, *r* represents the whole set of the atomic coordinates, and R is the lattice vector of the z-z-SWCNT structure, N corresponds to the number of cells in the z-z-SWCNT crystal in the reciprocal space that includes all the different *k*-values uniformly distributed in the Brillouin zone according to the applied periodic boundary conditions.[23-25] The geometries of the ligands (z-z-SWCNT and ATP) were then optimized, using the semiempirical AM1 method as implemented in MOPAC.[24,23]

Molecular Docking

In this work, a molecular docking procedure was performed to ascertain the interactions between the ATP-entry-point in hVDAC1 and its ligands (ATP and z-z-SWCNT). For this purpose, two different complexes were studied: ***i***) hVDAC1 with the z-z-SWCNT ligand (z-z-SWCNT/hVDAC1), ***ii***) hVDAC1 with the ATP ligand (ATP/hVDAC1)

First, the X-ray structure of the receptor was retrieved from the *RCSB Protein Data Bank* (PDB).[23] This corresponds to the PDB entry 2jk4 with a resolution of 4.1 Å. This structure was then refined,

by removing the water molecules and any other co-crystallized ligands. Additionally, hydrogen atoms were added to the hVDAC1 structure based on Gasteiger-Marsili empirical atomic partial charges, protonation states, bond orders and rotatable bonds.[26] To avoid obtaining false positives in the docking experiments, a hVDAC1 receptor structural validation was carried out through the Ramachandran maps of its ATP-entry-point residues.[33] This procedure allows verifying the absence of restricted flexibility for each of the hVDCA1 residues based on the allowed ψ *vs.* ϕ dihedral torsion angles of a given ATP-entry-point residue.

Before the docking runs, the potential hVDAC1-binding-sites including the ATP-entry-point were predicted using DeepSite.[28] This procedure was performed here by delimiting the van der Waals surface area of the ATP-entry-point binding residues, which bind to small ligands such as ATP or z-z-SWCNT. The DeepSite algorithm is based on a 3D-deep convolutional neural networks (DCNNs)[29-30] and was validated using more than 6500 proteins from the scPDB database.[27-28] The resulting ATP-entry-point docking box[32] was predicted to have a cubic form with size 16 Å and to be centered in the Cartesian point (X = 49.165 Å, Y = 13.086 Å, Z = – 6.072 Å).

All the molecular docking runs were performed using the AutoDock Vina package, with a Vina scoring function implemented ~~there~~ by Trott and Olson.[16, 26]

Several docking runs starting from random orientations (or conformations) of the z-z-SWCNT ligand interacting with the ATP-entry-point of hVDAC1 were executed and ranked according to their stability in terms of the estimated free energy of binding.

In order to give reliable results an exhaustiveness parameter equal to 100 (representing 100 z-z-SWCNT conformations) was established,[16, 26] which determines the number of search to find best crystallographic ligand conformation in the docking complex formed with the ATP-entry-point from "human protein" (*i.e.,* hVDAC1 crystallographic .pdb model).

The docking results were found as energetically unfavorable when the FEB values were lower or equal than 0 kcal/mol (worst crystallographic poses), clearly denoting either an extremely low or complete absence of affinity related to a repulsive pattern of interactions. Notice that the FEB of such complexes was computed considering a cutoff value of 7 Å for the interatomic distances $d_{i,j}$ between the *i*-ligands (z-z-SWCNT or ATP) and *j*-target residues of the ATP-entry-point, *i.e.*, only atoms with distances $d_{ij} \leq 7$ Å were considered as interacting atoms.[29-31] Moreover, the best root-mean-square deviation (RMSD; eq **3**) was stored as a criterion of correct docking pose accuracy for atomic positions below 2 Å.[29-30, 32-34]

$$RMSD = \sqrt{\frac{\sum_{i=1}^{n_L}\sum_{j=1}^{n_P}\left(x_i - x_j\right)^2 + \left(y_i - y_j\right)^2 + \left(z_i - z_j\right)^2}{n_L \times n_P}} \qquad \textbf{(3)}$$

In equation (3), n_L is the number of atoms of the ligand and n_P is the number of atoms of the hVDAC1 protein. Additionally, each term included in the double summation represents the distance between a ligand atom i with Cartesian coordinates (x_i, y_i, z_i) and a protein atom j with Cartesian coordinates (x_j, y_j, z_j).

ENM-ANM approach.

The elastic normal mode with anisotropic network models (ENM-ANM) is a computational approach which evaluates the degree of perturbation (strength of interactions), induced by a given ligand (z-z-SWCNT or ATP) in the residues network of a given protein (ATP-entry-point of hVDAC1), by describing the interaction potential (V) for a receptor-ligand complex as a Hookean potential (or 'springs') based on elastic normal mode analysis.[19-22] The mathematical framework of this approach has been extensively reported, and thus we will highlight only the more important aspects.

The ANM approach was performed, for each C(α)-atom of the N-terminal-(α)-helix residues, in the absence or presence of ligands.[18-22] Two VDAC1-residues were assumed to be in contact when their C(α)-atoms are separated by less than a cutoff distance (Rc ≈ 7 Å), which is directly related to effective communication distances ($^{\text{eff}}S_{(ij)} < 3{,}81$ Å) between C(α)-atoms of consecutively connected (i,j)-residues. The latter are identified by the mean-square distance traveled by a random walk of n-Markov transition steps according to the following equation,

$$(^{\text{eff}}S_{(ij)})^2 = n(L)^2, \qquad \textbf{(4)}$$

where L is the average step size.

The N-terminal α-helix residues were then represented as a transition matrix network that is controlled by Markov transition probabilities for the passage of information across the nodes (C(α)-atoms-hVDAC1-residues) to express the intrinsic fluctuation in the N-terminal-(α)-helix segment.[17]

The influence of ligands on the hVDAC1 inter-residue communication (N-terminal-(α)-helix segment) ~~are~~ is evaluated by a local-perturbation response scanning (LPRS) analysis, in which the perturbation strength that each protein residue has over every neighbor's residue is based on linear response theory.[19-22]

The collective fluctuation of the anisotropic network is completely ~~fully~~ defined by a $3N \times 3N$ Hessian matrix (H),

$$H_{i,j} = \begin{bmatrix} H_{1,1} & H_{1,2} & \ldots\ldots\ldots\ldots & H_{1,N} \\ H_{2,1} & H_{2,2} & \ldots\ldots\ldots\ldots & H_{2,N} \\ . & . & \ldots\ldots\ldots\ldots & . \\ H_{N,1} & H_{N,2} & \ldots\ldots\ldots\ldots & H_{N,N} \end{bmatrix} \quad \textbf{(5)}$$

in which its N-elements ($1 \leq i, j \leq N$) are the second derivatives of the anisotropic network potential (V):

$$H_{i,j} = \begin{bmatrix} \partial^2 V / \partial X_i \partial X_j & \partial^2 V / \partial X_i \partial Y_j & \partial^2 V / \partial X_i \partial Z_j \\ \partial^2 V / \partial Y_i X_j & \partial^2 V / \partial Y_i \partial Y_j & \partial^2 V / \partial Y_i \partial Z_j \\ \partial^2 V / \partial Z_i X_j & \partial^2 V / \partial Z_i \partial Y_j & \partial^2 V / \partial Z_i \partial Z_j \end{bmatrix} \quad \textbf{(6)}$$

On the other hand, the $3N$-dimensional vector $\Delta R(i)$ represents the residue displacements of hVDAC1 in *response* to the application of a *perturbation* induced by the ligand (*i.e.*: following Hooke's law), and can be represented by,

$$\Delta R(i) = H^{-1} F^{(i)}, \quad \textbf{(7)}$$

where the strength of perturbation ($F^{(i)}$ exerted on residue (i)) is expressed according to:

$$F^{(i)}{}_{1\times 3N} = \{0 \quad 0 \quad 0 \quad \cdots \quad F_x^{(i)} \quad F_y^{(i)} \quad F_z^{(i)} \quad \cdots \quad 0 \quad 0 \quad 0\}^{\mathrm{T}} \quad \textbf{(8)}$$

Once it has been set up, it is possible to obtain the inverse of the H-matrix ($H_{i,j}{}^{-1}$) according to the following equation:

$$H = \frac{1}{H_{i,j}} = -\frac{1}{s_{i,j}^{p+2}} \begin{bmatrix} (X_j - X_i)(X_j - X_i) & (X_j - X_i)(Y_j - Y_i) & (X_j - X_i)(Z_j - Z_i) \\ (Y_j - Y_i)(X_j - X_i) & (Y_j - Y_i)(Y_j - Y_i) & (Y_j - Y_i)(Z_j - Z_i) \\ (Z_j - Z_i)(X_j - X_i) & (Z_j - Z_i)(Y_j - Y_i) & (Z_j - Z_i)(Z_j - Z_i) \end{bmatrix} \quad \textbf{(9)}$$

($H_{i,j}{}^{-1}$) may be used to predict the auto- and cross-correlations of residues, and it represents the covariance matrix of *3N* multi-variant distribution. This matrix holds the relevant information on the hVDAC1-residues fluctuations (*i.e.,* the residues from ATP-entry-point involved in the formation of stable ligand/hVDAC1 complexes): ~~and~~ $s_{i,j}$ represents the instantaneous distance between nodes or residues (i and j); and p is an empirical parameter.[19-22]

The main idea in the this LPRS analysis is to represent quantify? the force of the ligand-perturbations on the target-residues of ATP-entry-point to detect the response of the overall network

following **eq 7**. As mentioned above, $\Delta R\ (i)$ is a *3N*-dimensional vector that describes the displacements of all the residues (*i.e.,* in *N*-blocks of dimension 3, each) under perturbation $F^{(i)}$.[22] The response of a given *k*-residue is the magnitude $\left\langle \left\| \mathbf{\Delta R}_k^{(i)} \right\|^2 \right\rangle$ of the k^{th} block of $\Delta R\ (i)$ averaged over multiple $F^{(i)}$, expressed as an element of the $3N \times 3N$ LPRS matrix.[22]

The response to local displacements at each perturbation site is obtained by dividing each row by its diagonal value (*d*) as shown in the following equation,

$$\overline{\boldsymbol{S}}_{\text{LPRS}} = \begin{pmatrix} 1/d_1 & 0 & 0 \\ 0 & \ddots & 0 \\ 0 & 0 & 1/d_N \end{pmatrix} \text{LPRS}, \qquad \textbf{(10)}$$

where each i^{th} row of $\overline{S}_{\text{LPRS}}$ refers to the profile generated by the perturbing residue (*i*).

Molecular Dynamics Simulations.

To understand the interactions between ligands and hVDAC1 (ATP-entry-point) at nanometric level, we performed MD simulations for three different systems, *i.e.*: ATP-hVDAC1, z-z-SWCNT-hVDAC1 and ATP-z-z-SWCNT-hVDAC1 combined structures. The initial structures of the ligand-hVDAC1 were taken from the molecular docking results and placed each of them at the center of a three-dimensional periodic cubic box with size 8.9 nm x 8.9 nm x 8.9 nm. Afterwards, the boxes were filled with 21,910 water molecules, and few Cl^- ions were added to neutralize the systems.

The GROMACS-5.1.4 software package[35-36] was used for performing all the MD simulations. The intra- and inter-molecular interactions of the ligand-hVDAC1 protein were modeled by the GROMOS 43A1 force field parameter set, [37-38] and the water molecules by the SPC/E potential[39] with rigid bonds and angle. The cross interactions between unlike atoms were calculated by applying geometric combination rules.[40-42] The steepest descent algorithms were used for 50000 steps to optimize the initial geometry keeping the ligand-hVDAC1 complex rigid.

Thereafter, systems were equilibrated in two steps: **1)** the systems were simulated for 100 ps in NVT ensemble (number of atoms volume and temperature constant) to stabilize the system's temperature at 300 K, **2)** the systems were then equilibrated for 100 ps in NPT ensemble (number of atoms, pressure and temperature constant) to stagnate the pressure of the systems at 1 bar. After these equilibration steps, MD simulations were performed for 20 ns in *NPT* ensemble to collect data for analysis. This production run was considered appropriate, once it was observed the distance between the center of mass of the ATP-entry-point and the center of mass of the ligand's constant for first 6 ns of the production run. The leap-frog algorithm[43], with a time step of 2 fs, was employed to integrate the equation of motion for the systems. The system pressure was controlled

by a Parrinello-Rahman method[44] with a time constant of 2.0 ps, and the system temperature was kept close to the intended value of 300 K, using the v-rescale coupling algorithm[45] with a time constant of 0.1 ps. The cut off distance for both the Lennard-Jones potential and short-range Coulombic interactions were 1 nm.[46] The long-range Coulombic interactions were calculated by the Particle Mesh Ewald (PME) method.[47-48]

The binding free energy of the complexes was calculated using the Molecular Mechanics Poisson Boltzmann Surface Area (g_mmpbsa) method implemented in GROMACS 5.1.4.[49] The binding free energy of the complexes was analyzed by taking trajectory frames at an interval of 1 ps of the simulations. The binding free energy can be expressed as follows,

$$FEB \approx \Delta G_{bind} = G_{complex} - \left(G_{hVDAC1} + G_{ligand}\right) \quad \textbf{(11)}$$

where $G_{complex}$ is the total free energy of the ligand/hVDAC1 (ATP-hVDAC1, z-z-SWCNT-hVDAC1 or ATP-z-z-SWCNT/hVDAC1) complex, and G_{hVDAC1} and G_{ligand} are the total free energy corresponding to the separately solvated hVDAC1 and ligand (ATP, z-z-SWCNT or ATP-z-z-SWCNT), respectively. The free energy ($G(x)$) for each individual species x (ligand, hVDAC1 or ligand/hVDAC1 complex) can be expressed as depicted in equations **11** and **12**.

$$G(x) = \left\langle E_{MM}(x) \right\rangle - T\,S(x) + \left\langle G_{solvation}(x) \right\rangle \quad \textbf{(12)}$$

$$E_{MM}(x) = E_{bonded}(x) + E_{nonbonded}(x) = E_{bonded}(x) + E_{vdw}(x) + E_{elec}(x) \quad \textbf{(13)}$$

In equation (13), $\langle E_{MM}(x) \rangle$ is the average molecular mechanics potential energy of the molecular specie x, $S(x)$ is the respective entropy and $\langle G_{solvation}(x) \rangle$ is the average value of its solvation free energy. According to equation (8), the potential energy ($E_{MM}(x)$) can be expressed as the sum of its bonded ($E_{bonded}(x)$), van der Waals ($E_{vdw}(x)$) and electrostatic ($E_{elec}(x)$) components. The solvation free energy ($G_{solvation}(x)$) is expressed as the sum of the polar ($G_{polar}(x)$) and nonpolar ($G_{apolar}(x)$) solvation free energies according to the following equation,

$$G_{solvation}(x) = G_{polar}(x) + G_{apolar}(x), \quad \textbf{(14)}$$

where $G_{polar}(x)$ is estimated solving the Poisson-Boltzmann equation and $G_{apolar}(x)$ is calculated from the solvent accessible surface area ($SASA(x)$) using the following expression,

$$G_{apolar}(x) = \gamma SASA(x) + b, \quad \textbf{(15)}$$

where γ and b are the empirical constants.

Results and discussion

Ligand selection, characterization and modeling of z-z-SWCNT.

Let us first start by focusing on the well-known direct proportionality relationship between the carbon nanotube zig-zag geometry with the nanotoxicity-based reactivity at the subcellular level (mitochondria).[12-13] The presence of dangling bonds in the tip of the z-z-SWCNT has a direct influence on the modeled biochemical response (*i.e.,* mitochondrial channel nanotoxicity). Herein, we select the zig-zag topology (Hamada index $m = 0$, $n > 0$) like a robust and recognized electro-topological nanodescriptor of single-walled carbon nanotube ligand (z-z-SWCNT). Because, it is well known that the potential mitochondrial channel nanotoxicity properties of z-z-SWCNT are greater compared to its non-zig-zag geometric counterparts as amchair-SWCNT (Hamada index $m = n$) and chiral-SWCNT, when it has Hamada index (n, m), with $m > 0$ and $m \neq n$; and its enantiomer (or mirror image) has Hamada index (m,n), which is different from (n, m) no reflection symmetry.[12-13]

As reported in previous studies, a unique phenomenon of "edge effects" present only in semiconducting pristine z-z-SWCNT geometries has paramount importance like structural nanodescriptor of mitochondrial channel nanotoxicity.[12-13] Indeed, the presence of tip-charge variations in the open z-z-SWCNT-extremes from the cycloparaphenylene aromatic system; increases the reactivity of these carbon nanotubes when compared with their non-zig-zag geometric counterparts like armchair-SWCNT and chiral-SWCNT.[12-13] Besides, the influence of dangling bonds in the z-z-SWCNT tested, induce appreciable changes in the structural and electronic properties of the z-z-SWCNT system, partially mimicking the effects of topological vacancies observed in the SWCNTs with side-wall defects. It is well known that the z-z-SWCNT dangling bonds can influence the Fermi energy. In fact, the existence of more sp^3-C-atoms can induce a flat-band magnetism (magnetic polarization) in the Fermi level, that together with the π-electrons produce a larger increase in the intrinsic reactivity of the z-z-SWCNT topologies, maximizing the nanointeractions and consequently its mitochondrial channel nanotoxicity (*i.e.*, more negative expected FEB values obtained from docking and molecular dynamic simulations) compared its non-zig-zag geometric counterparts (amchair-SWCNT and chiral-SWCNT).

In this context, it is important to note that during biochemical interactions of a given pristine-SWCNT with mitochondrial redox-components, dangling bonds formation from non-zig-zag geometric counterparts (amchair-SWCNT and chiral-SWCNT) can also be spontaneously generated at the subcellular level (mitochondria).

Then, we performed the ligand selection, modeling and characterization of the electronic structure using a validated z-z-SWCNT (8.0) ligand model to ensure the quality of our nanotoxicological predictions on hVDAC1 (ATP-entry-point).[12-13]

Herein, we present the results of the modeled z-z-SWCNT (8.0) ligand used in our study, which was obtained by using the reciprocal ZF scheme introduced by Saito and Dresselhaus,[24-25] which is considered a good approximation for 2D Brillouin zone of graphene, within the tight-binding electronic band structure approach when applying Wannier orthogonal functions (see **Figure 1**).[23-25]

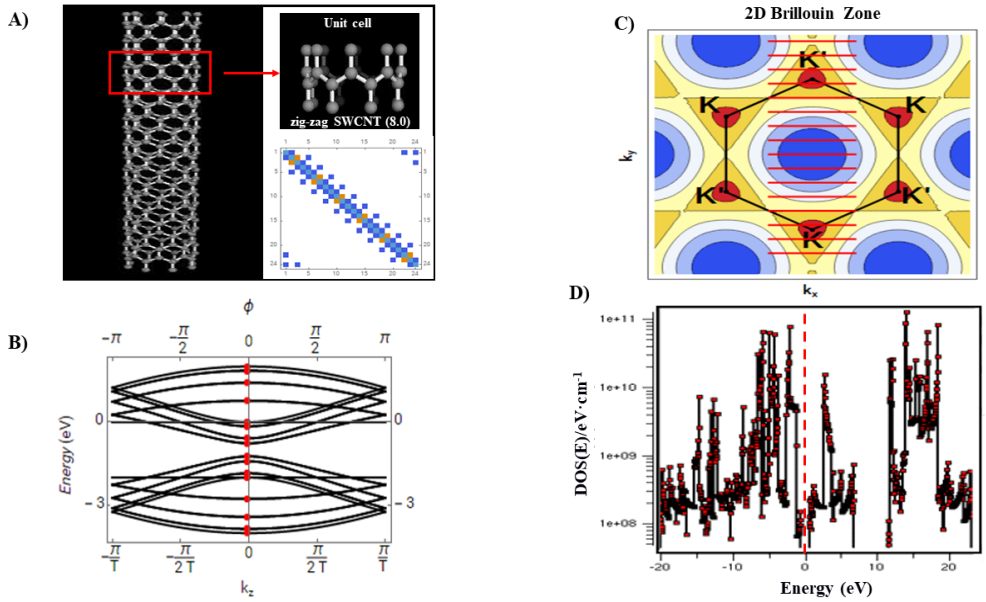

Figure 1. Electronic structure z-z-SWCNT obtained using the small crystal approach based on the reciprocal zone-folding (ZF) method with Wannier orthogonal functions. **A)** Molecular model used, with the corresponding unit cell showing an alternative way to depict the reciprocal space zone-folding (ZF) like a tight-binding Wannier representation. **B)** Electronic band structure representation of Energy (eV) *vs*. k_z, performed by ZF method setting the following tight-binding parameters: hopping parameter $t = -1$, on-site energy parameter $\epsilon = -1$ and overlap $s = 0$. **C)** Contour plot, for the 2D Brillouin zone, obtained by applying the ZF method in the 2D-graphitic Brillouin zone with Dirac points (K and K′) uniformly distributed (red cutting lines) in the (k_x, k_y)-plane. **D)** Representation of the density of electronic states (DOS) profile as a function of the energy (E) counting all over the states within each interval $[E, E + dE]$.

Molecular docking. A key step to ensure the accuracy of molecular docking data involves the correct prediction of suitable ATP/hVDAC1 binding sites. Many algorithms for detecting protein-binding cavities have been settled over the years based on the crystallographic structure, geometric, and chemical protein 3D-features (ATP/hVDAC1). In the present study, the prediction of the binding residues from hVDAC1 (the ATP-entry-point) was carried out using the machine learning

algorithm based on 3D-deep convolutional neural networks (DeepSite-CNNs chemoinformatic tool), [50] which was previously validated by an extensive test set from the scPDB database (> 7000 proteins structures).[51-52] The structural identification results thereby obtained for the hVDAC1 binding-sites including the ATP-entry-point are presented in **Figure 2**.

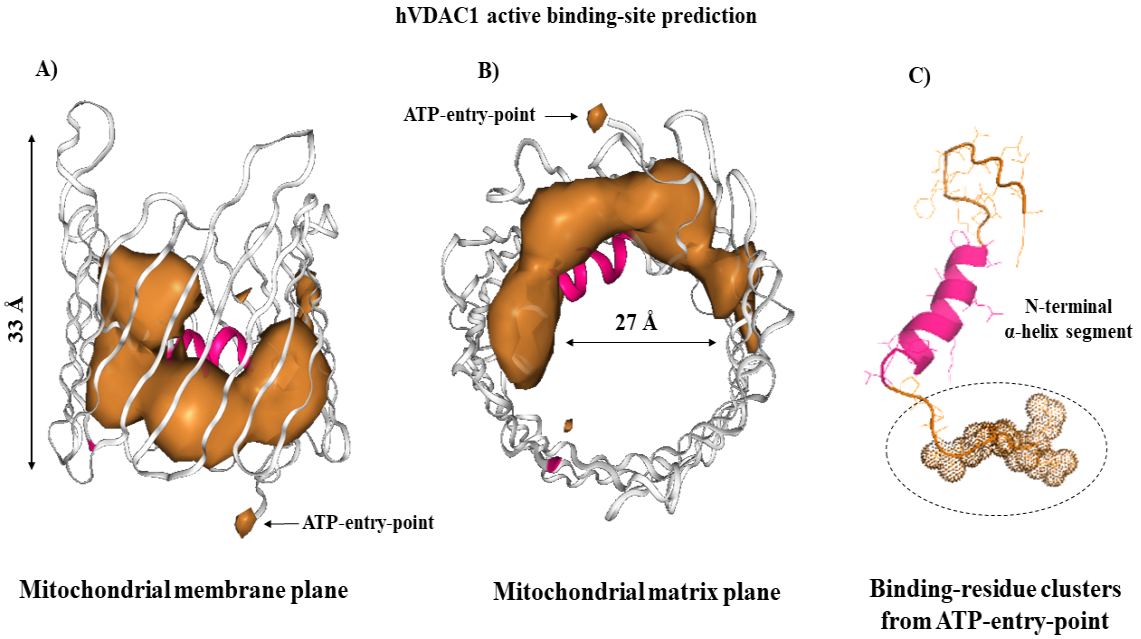

Figure 2. **A)** DeepSite prediction of topological cavities of the hVDAC1 active binding sites (volumetric orange regions) from lateral view. **B)** Display of the hVDAC1active binding-sites (volumetric orange regions) from the mitochondrial matrix plane showing the ATP-entry-point. **C)** Representation of the N-terminal-(α)-helix segment including the binding-residue clusters (MET1, ARG2, GLY3, SER4, ALA5) of the hVDAC1 channel.

Following on, to validate the 3D X-ray crystallographic structure of the N-terminal α-helix segment a Ramachandran analysis was carried out. This analysis comprised plotting a 2D-projection on the plane of the 3D-crystallographic structure of protein hVDAC1, describing all possible conformations of the ATP-entry-point residues by considering the dihedral angles (ψ and ϕ) around the peptide-bond of such residues.[53] The allowed ψ *versus* ϕ torsion values of a given residue of hVDAC1, found within the Ramachandran purple colored contour, were considered as conformationally favored residues. Otherwise, those were considered as sterically disallowed residues (see **Figure 3**). As seen, the Ramachandran plot obtained corroborates the very good X-ray crystallographic quality of the N-terminal-(α)-helix segment model with an expected percentage > 90% for favored regions. It is also important to note that, the LYS23 and ALA11 (Ramachandran outliers) are not part of the ATP-entry-point.

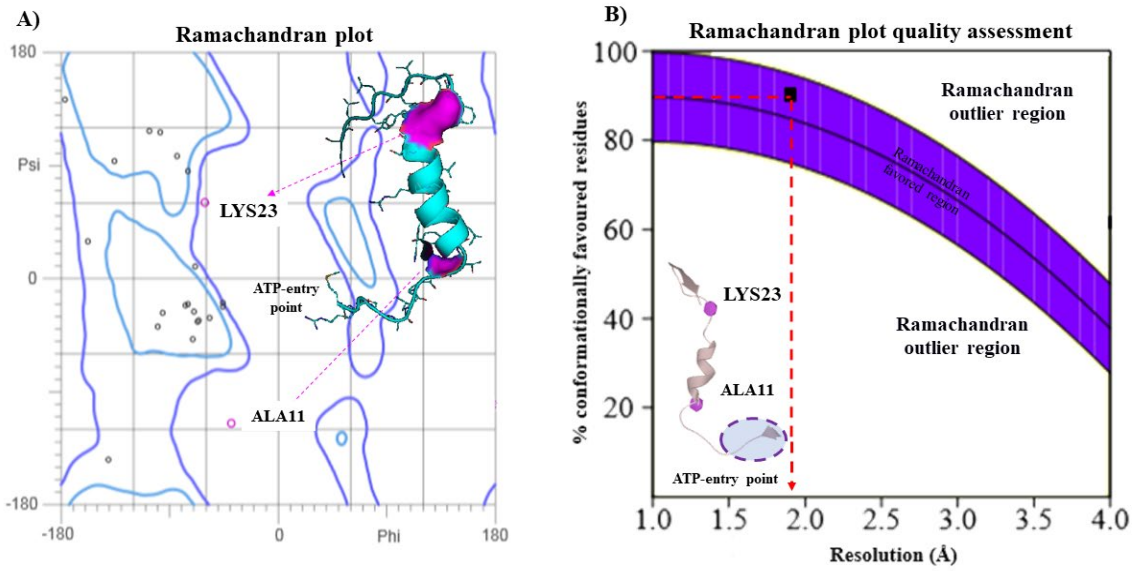

Figure 3. **A)** Ramachandran plot and spatial distribution of its outliers (light purple residues: ALA11 and LYS23) only for the N-terminal α-helix segment of the hVDAC1-channel PDB X-ray structure. All the possible combinations of Psi *vs.* Phi dihedral torsion angles of each amino acid residue of the hVDAC1-channel protein are shown. **B)** Ramachandran plot quality assessment (hVDAC1-channel model quality) measured by the percentage of the hVDAC1-residues that are in the most favored residues localized in the purple shaded region.

To elucidate the critical regions that could be affected by z-z-SWCNT-protein interactions, we evaluated also the flexibility properties of the hVDAC1 general structures considering the N-terminal-(α)-helix domain.[1-9] Particularly, it can be seen in **Figure 4** that the ATP-entry-point's flexibility properties are crucial to investigate the mitochondrial channel nanotoxicity-based bioenergetic dysfunction.

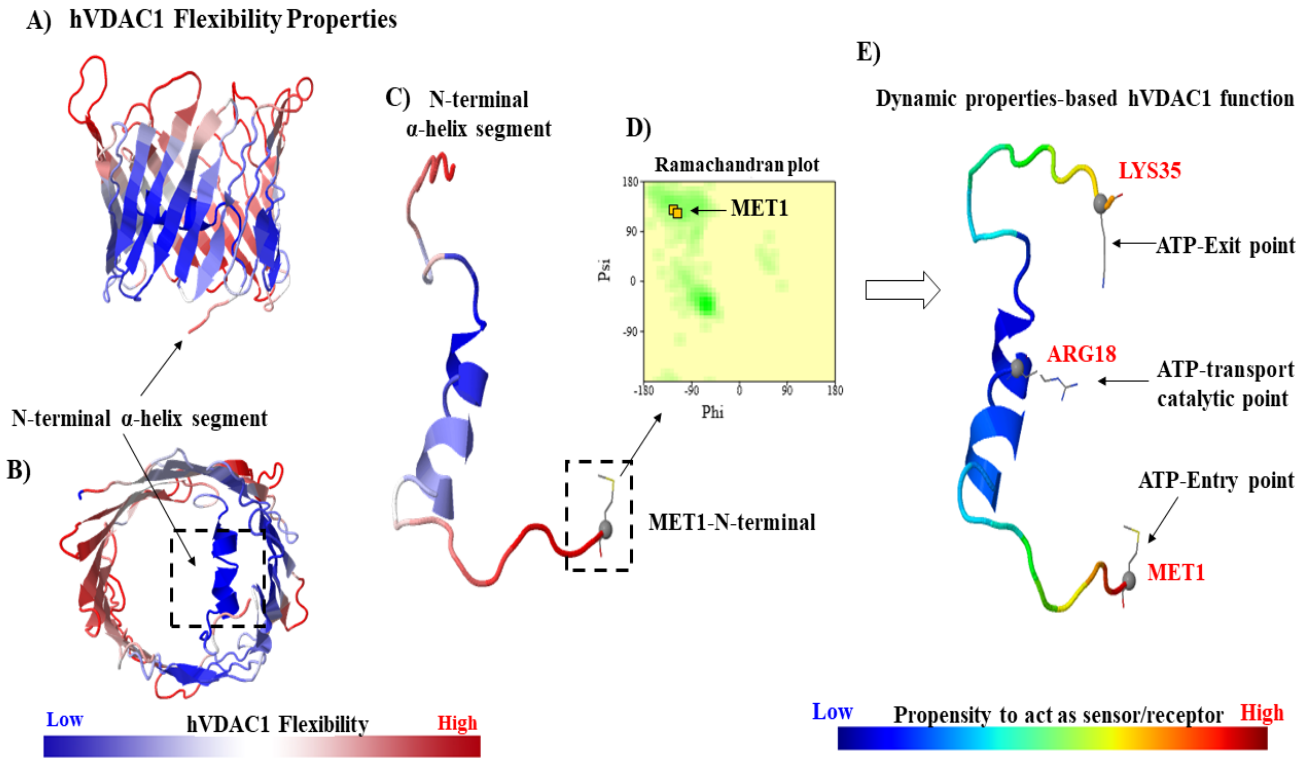

Figure 4. Schematic representation of the hVDAC1 flexibility properties. The colored structures are based on the size of fluctuations of the hVDAC1-residues showing low-flexibility (blue) to high-flexibility (red). **A)** Lateral view of hVDAC1. **B)** Mitochondrial matrix plane view of hVDAC1. **C)** The flexibility properties of N-terminal-(α)-helix segment including the MET1-flexibility corresponding to the first residue of the ATP-entry-point. **D)** Ramachandran validation based on ψ *vs.* ϕ dihedral torsion angles for the first ATP-entry-point residue (MET1) with allowed conformational properties (inner light green region). **E)** Representation of the N-terminal-(α)-helix based on hVDAC1 dynamic functional properties. Herein, it shows the behavior (like effector or sensor) of the most critical residues of the ATP-entry-point in the absence of z-z-SWCNT, such as MET1: effector-residue (red region), ATP-catalytic point ARG18 residue: sensor-residue (blue region), and the ATP-exit point LYS35 residue: chain A receptor-behavior (red region).

After this, we carried out the molecular docking experiments to obtain the Gibbs free energy of binding (FEB) for the three complexes under study. The results obtained show that the FEB values are very similar for the two binary complexes (–3.7 kcal·mol^{-1} for z-z-SWCNT/hVDAC1 and –3.8 kcal·mol^{-1} for ATP/hVDAC1). These results demonstrate the reliability of the proposed mechanism for the z-z-SWCNT channel-nanotoxicity, based on hydrophobic and electrostatic interactions established between this ligand and the ATP-entry-point residues.

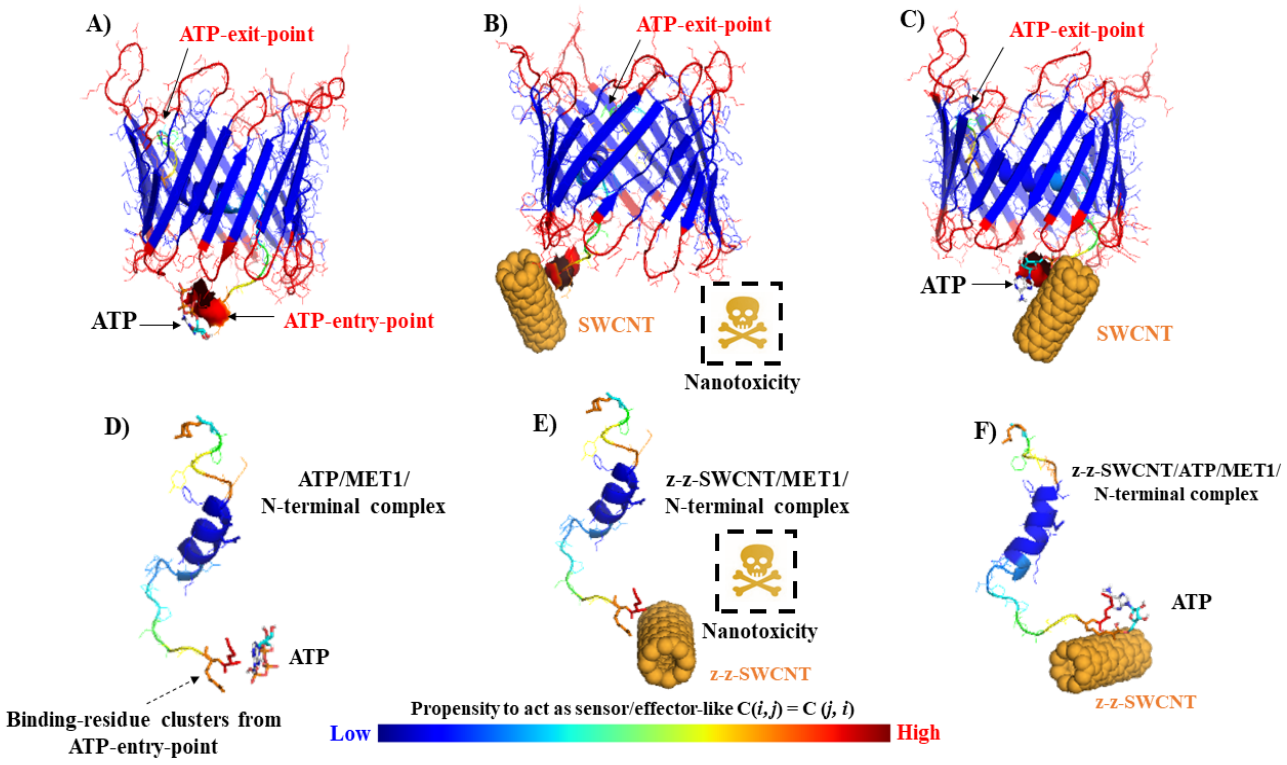

Figure 5. On the top row, snapshots showing the molecular docking results for the best binding-poses like: **A)** docking control ATP/hVDAC1 complex (–3.8 kcal/mol), **B)** z-z-SWCNT/hVDAC1 complex (–3.7 kcal/mol) and **C)** overlapping representation of the best binding-poses of ATP and the z-z-SWCNT at the ATP-entry-point. The ATP-entry-point residues (MET1, ARG2, GLY3, SER4, and ALA5) are depicted as small van der Waals surfaces labeled-red. In the bottom row, the docking complexes like **D)** ATP/hVDAC1, **E)** SWCNT/hVDAC1 and **F)** overlapping binding-poses of ATP and SWCNT are presented considering the best binding-poses of these ligands interacting simultaneously with the ATP-entry-point from the N-terminal-(α)-helix segment

The docking results, depicted in **Figure 5**, suggest that the interactions between z-z-SWCNT and the ATP-entry-point residues are hydrophobic. Furthermore, it is important to highlight that the regulatory SER-(4)-N-terminal α-helix residues have an important role in the phosphorylation mechanism for controlling the function of ATP-entry. The presence of z-z-SWCNT could significantly weaken the physiological function pathways and induce post-translational modifications in SER4.[12, 18] It is well-known that hVDAC1 post-translational modifications are associated with biochemical reactions of phosphorylation. According to this, we thus suggest that the z-z-SWCNT might mimic pathological conditions like post-translational modifications in the SER4 of the ATP-entry-point such as metabolic stress, aging, cancer, and cardiovascular diseases.[6] Furthermore, it resembles that z-z-SWCNT initially blocks the ATP-transition from the first residue (MET1) of the ATP-entry-point before it interacts with the positively charged ε-amino groups (N^+

primary amines) of ARG2-hVDAC1. The amino groups (N^+) of ARG2-hVDAC1 are highly reactive and often participate in reaction at the ATP-entry-point acting as a voltage sensor in mitochondria.[4, 18] Nevertheless, the presence of z-z-SWCNT and ATP molecules in the same biophysical environment could induce local-perturbations in the inter-residue communication, and the transduction properties of the ATP-entry-point. This would affect the signal communication efficiency in the N-terminal-(α)-helix segment and the subsequent steps of the ATP-translocation through hVDAC1 like ATP-transport in the catalytic point (ARG18) and the ATP-efflux point (LYS35).[7-9] Overall this thus suggest that the molecular docking mechanism is likely-based on local-perturbations (interactions) with effector and allosteric residues from the ATP-entry-point.[19]

To further evaluate the local perturbation on ATP-entry-point residues in the absence or presence of ligands (z-z-SWCNT and ATP-native substrate of VDAC), we applied an anisotropic network approach based on the biophysical parameter Markov commute-time [C (*i, j*) →C (*j, i*)].[19,54] The latter represents the ability of a given target to receive (sensor residues) or send (effector residues) perturbation signals in both directions (*j*→*i* and *i*→*j*). See **Figure 6**.

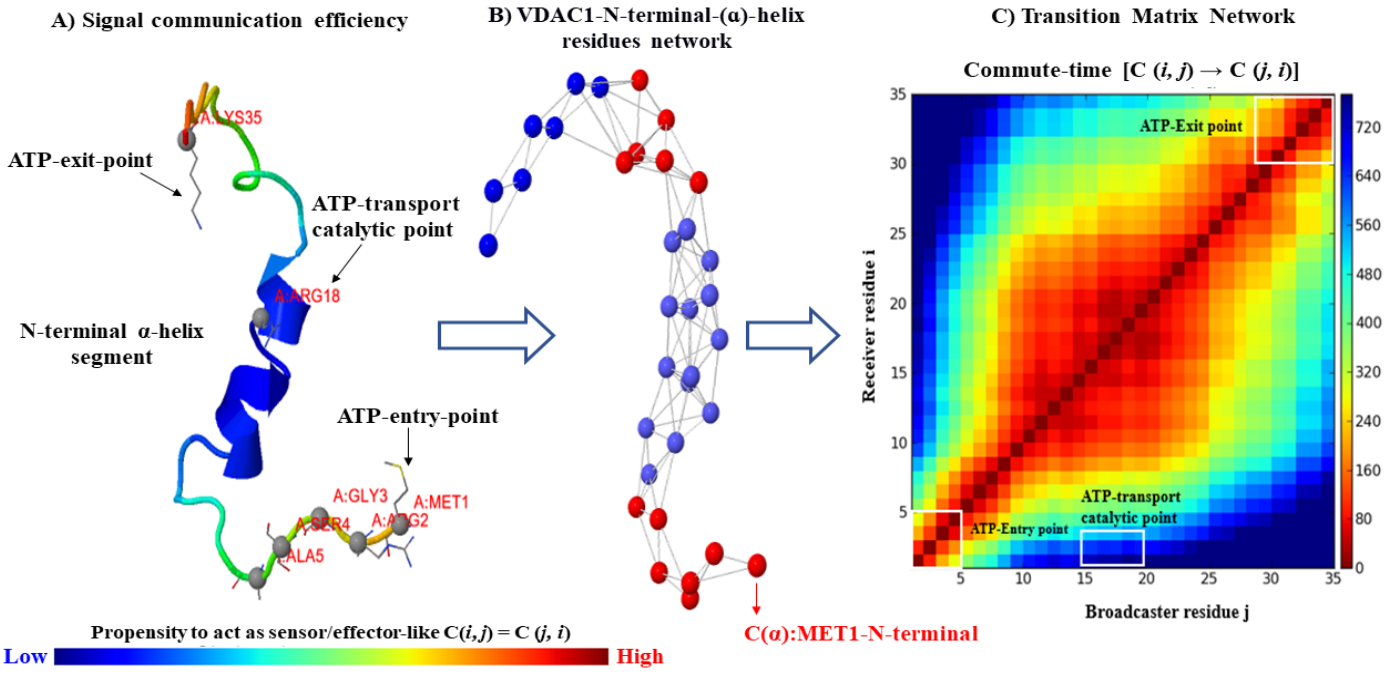

Figure 6. **A)** Representation of intra-molecular communications between residue's fluctuation in the N-terminal-(α)-helix segment based on the efficiency of sensors (blue) and effectors (red): ***i***) ATP-entry-point ***ii***) ATP-transport in the ATP-catalytic-point (ARG18) ***iii***) ATP-exit-point (LYS35) **B)** N-terminal-(α)-helix residues network of C(α)-atoms connected by elastic springs. Herein, the color of atoms (spheres) is depicted depending on the B-factor. **C)** Two-dimensional transition matrix network-based on the Markov commute time (C (*i, j*)), clustering sensor and effector residues in the N-terminal-(α)-helix. The critical regions of ATP-transport stages are represented by white rectangles. The color bar on the right side indicates low (blue) and high (red) commute time.

Following this idea, we theoretically modeled the local-perturbation response induced by the ligands in the ATP-entry-point. The results of this local-perturbation response scanning analysis are presented in **Figure 7**.

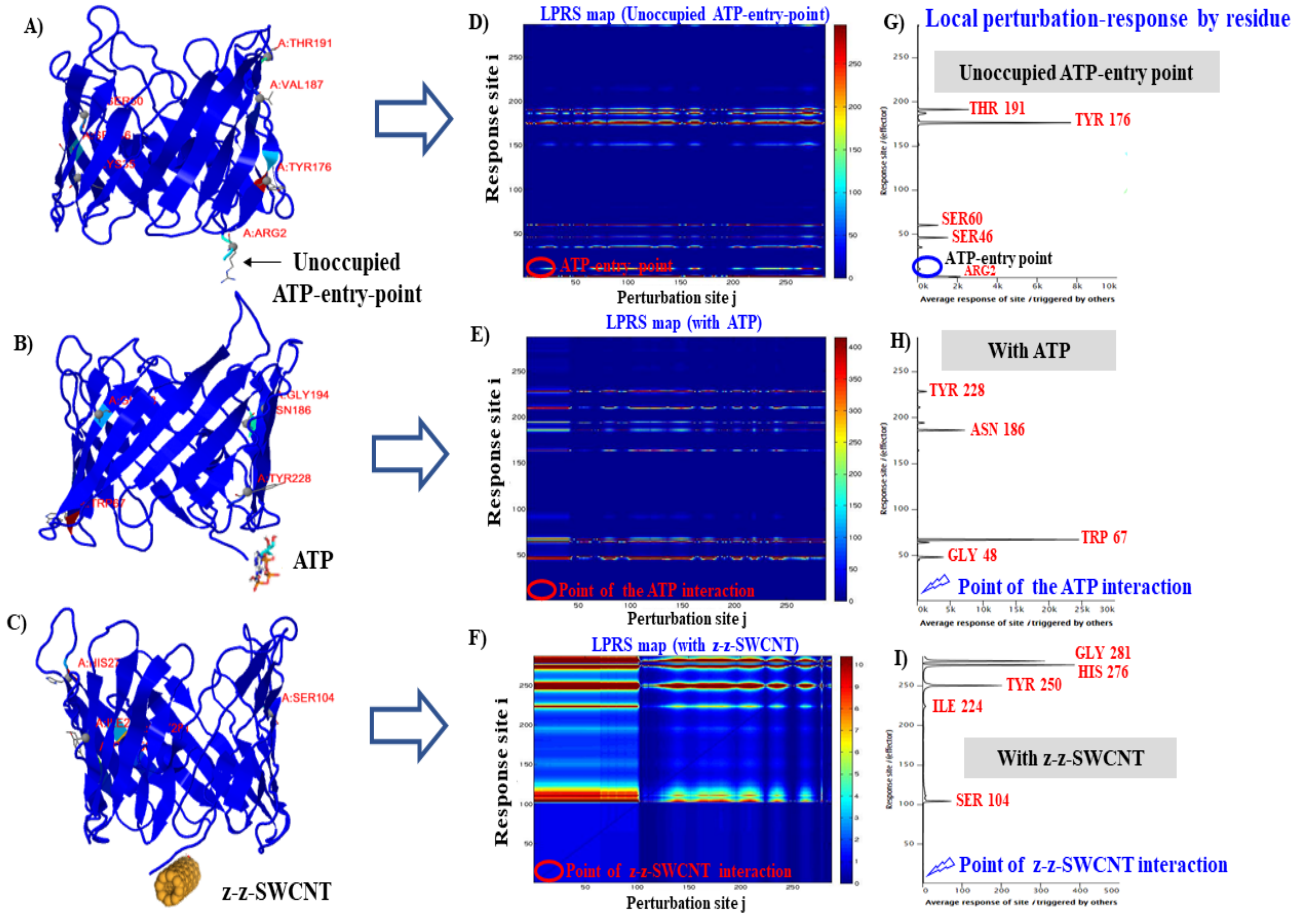

Figure 7. On the left, 3D-cartoon representations for the simulated conditions, namely: **A)** hVDAC1 without ligand, **B)** ATP/hVDAC1 complex, and **C)** z-z-SWCNT/hVDAC1 complex. On the right, the corresponding local perturbation-response scanning (LPRS) analysis showing the $\overline{S}_{\text{LPRS}}$-matrix perturbations from (*j*)-sensors residues *vs.* (*i*)-effector residues based on the previously defined strength of perturbations as indicated by the scales on the right of the maps. The subfigures in the central column represent LPRS analysis results for: **D)** hVDAC1 without ligand, **E)** ATP/hVDAC1 complex, **F)** z-z-SWCNT/hVDAC1 complex considering the best binding-conformation for both ligands in hVDAC1, **G)** hVDAC1 without ligand, **H)** ATP/hVDAC1 complex, and **I) z-z-**SWCNT/hVDAC1 complex. The regions blue to orange correspond to weak to moderate local perturbations whereas the regions orange to dark red to strong ones in the ATP-entry-point inter-residue communication (*i*, *j*).

The behavior of the local perturbation response of (*i*)-hVDAC1 effector residues provides relevant information regarding the effective communication distances ($^{\text{eff}}S_{(ij)}$) for intra-segment Cα-Cα atomic distances, which can be categorized as: *i)* short segments (10–22 residues), *ii)* medium segments (23–26 residues), and *iii)* long segments (27–50 residues) in the N-terminal-(α)-helix

segment.[55] Considering the results of local perturbation response of (*i*)-hVDAC1 effector residues in the presence and absence of ligands (z-z-SWCNT and ATP), it appears that z-z-SWCNT affects the inter-residue communication of the ATP-entry-point residues following a long distance-perturbations response, affecting allosteric-phosphorylation residues like SER 104 and TYR 250 or other as HIS 276 and GLY 281. Even though the ATP-ligand has a similar long-distance perturbation response, but the perturbed-residues were different (like GLY 48, TRP 67, ASN 186 and TYR 228). Also, the interaction pattern of z-z-SWCNT is significantly different regarding the physiological condition from the unoccupied ATP-entry-point residues, and the effector-residue like ARG 2 keeps its flexibility properties.

Molecular dynamics results. Presently, computational approaches to model channel nanotoxicity have paramount importance in mitotarget drug-discovery and rational-design of carbon nanomaterials (SWCNT).[12-13] Previous theoretical and *in vitro* studies have demonstrated that SWCNT can induce mitochondrial toxicity with special selectivity by the mitochondrial channels.[56-57] In this context, computational methods like MD can efficiently model with good accuracy many protein-ligand complexes based on the prediction of binding conformations and affinities (FEB values) between drug molecules (*i.e*., the native hVDAC1-substrate ATP and the z-z-SWCNT) and the mitotarget (*i.e*., ATP-entry-point). Herein, it is important to note that the *in silico* nanotoxicological assays correspond to a very early stage of the nano-risks evaluation. Therefore, several approximations are adopted in the new field of "Computational Nanotoxicology" during the simulations (modeling z-z-SWCNT/hVDAC1-channel nanotoxicity). In this context, we assume that the probability of occurrence of potential off-target z-z-SWCNT/hVDAC1-interactions with lipid bilayers of cell membranes (including the lipid bilayers of mitochondria membranes as outer-and-inner mitochondrial membranes) in the biological environment could be considered from medium to low. As mentioned in the **Introduction** section the hVDAC1 channel is the most densely localized protein in the outer mitochondrial membrane of all human cells,[1, 8-10] and on the other hand, the SWCNT (z-z-SWCNT) present high ability to accumulate in the mitochondrial matrix (mitotropic behavior). According to this, several steps biochemical could bring on potential off-target hVDAC1-interactions of z-z-SWCNT with the lipid bilayers of mitochondria membranes like: i) z-z-SWCNT first pass across the outer mitochondrial membrane, where the hVDAC1 channel is embedded. ii) The second pass is the arrival of z-z-SWCNT to the mitochondrial inter-membrane space following by iii) the passage of z-z-SWCNT to the mitochondrial matrix across the mitochondrial inner-membrane where the ATP-entry-point of hVDAC1 is placed in the facing-inward conformation in mitochondrial matrix.

Then, we show the initial and final MD configurations for the isolated ligand-hVDAC1 systems, where the water molecules and ions were excluded for a clearer view of ligands binding position in the hVDAC1 channel. In the case of ATP-hVDAC1 complex, the ATP molecule does not move much inside the hVDAC1 channel from its docking position, rather prefers to be close to the ATP-entry-point. On the other hand, for the z-z-SWCNT-hVDAC1 complex, we show that the z-z-SWCNT moves toward the hVDAC1 from its docking position during simulation and interacts strongly with the α-helix segment. The MD simulation results are depicted in **Figure 8**.

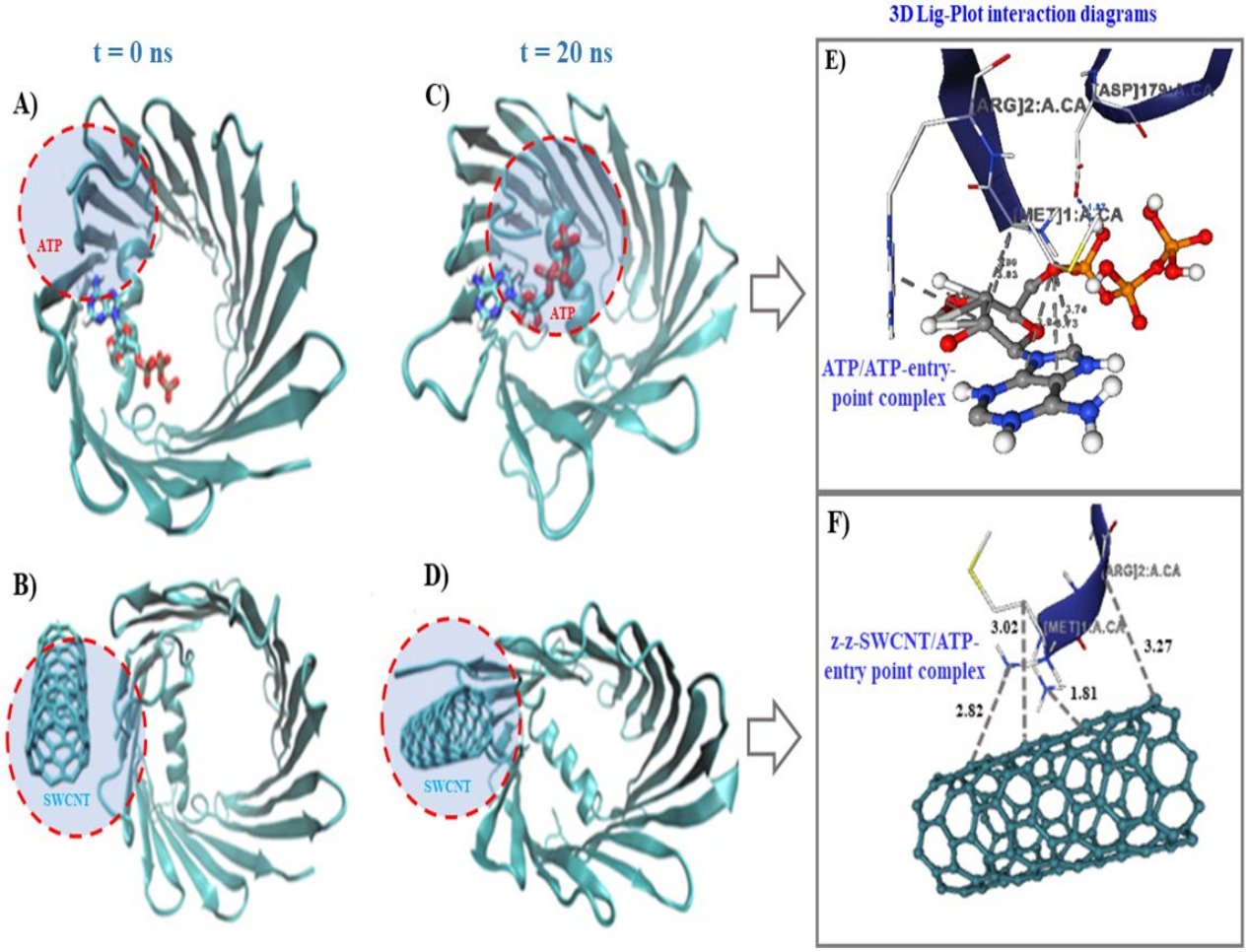

Figure 8. Snapshots of ligand-hVDAC1 complexes obtained from MD simulations (red dotted line). Herein, **A)** and **B)** represent snapshots of the ATP/hVDAC1 complex (marked by red circle) and the z-z-SWCNT/hVDAC1 (marked by red circle), respectively, at the beginning of the MD simulation (t = 0 ns), whereas **C)** and **D)** represent snapshots from the same complexes at the end of MD simulations (t = 20 ns). The diagrams, **E)** and **F)** represent the 3D-lig-plot hydrophobic interaction with the corresponding critical interatomic distance values ($d_{ij} \leq 7$ Å) from relevant residues of the ATP-entry-point depicted for the aforementioned docking complexes just considering the end of MD simulations (t = 20 ns).

To trace the ligand movement from its docked position in the complexes during the simulations, the distances between the center of masses (CM) of the ligand (z-z-SWCNT or ATP) and the ATP-entry-point were calculated and are depicted in **Figure 9.**

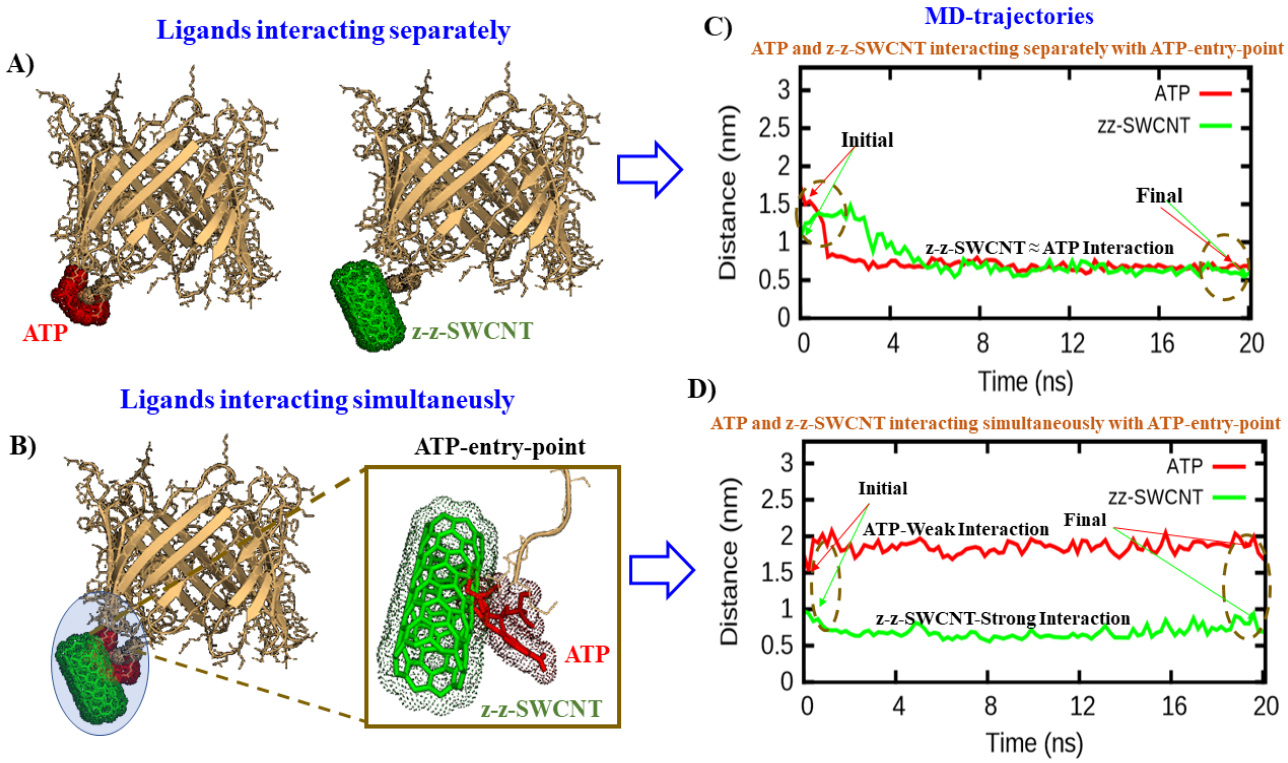

Figure 9. In the left column, 3D-molecular structures are represented for the simulated complexes, namely: **A)** ATP/hVDAC1 and z-z-SWCNT/hVDAC1 complexes, and **B)** Representation of the ATP molecule and the z-z-SWCNT ligand interacting in the same biophysical environment (ATP-entry point). In the right column, the calculated distances between the center of mass (CM) of the ligands and the CM of ATP-entry-point residues during 20 ns of MD simulations are presented. **C)** MD-trajectories-based distances of the ATP and z-z-SWCNT interacting separately with the ATP-entry-point and **D)** MD-trajectories-based distances of ATP and z-z-SWCNT interacting simultaneously with the ATP-entry-point.

This strategy allowed us to reveal important toxicological aspects based on the selectivity and/or affinity of z-z-SWCNT with mitochondrial channels (hVDAC1).[12-13, 58] According to the obtained results (see **Figure 9C**), the distance between the CM of ATP and the CM of ATP-entry-point in the ATP/ATP-entry-point system decreases from 1.7 nm to 0.65 nm during 20 ns simulation. Similarly, the distance between the CM of z-z-SWCNT and ATP-entry-point in the z-z-SWCNT/hVDAC1 system also decreases from its docked position suggesting a strong attractive interaction between the ligand and the ATP/ATP-entry-point. On the other hand, the distance between the CM of the ligands (ATP and z-z-SWCNT) and the CM of ATP-entry-point (see **Figure 9D**) in ATP+ z-z-SWCNT/hVDAC1 system remains almost absolute for both cases. But the distance between the CM of z-z-SWCNT and ATP-entry-point is much shorter than the distance between the CM of ATP

and ATP-entry-point, thus implying a stronger attractive interaction between z-z-SWCNT and the ATP-entry-point. This thus suggests that the z-z-SWCNT-toxicodynamic behavior (*i.e.*, proposed ligand interaction mechanism with the ATP-entry-point) could interfere with the ATP physiological function and in turn, directly affect the mitochondrial bioenergetic function in early stages of ATP-transport through hVDAC1 channel.[3-6]

To have a deeper understanding on the interaction of ligand/ATP-entry-point interactions, the respective free energy of binding (FEB) values were calculated using the Molecular Mechanics Poisson Boltzmann Surface Area algorithm implemented in GROMACS 5.1.4.[49] The obtained total Gibbs free energy of binding (FEB or E_{bind}) of ATP forming the ATP/hVDAC1 complex (−336.82 kcal/mol) presents more negative FEB values, indicating a higher interaction affinity than ATP in the presence of z-z-SWCNT forming the complex of z-z-SWCNT+ATP/hVDAC1 with a FEB = −277.24 kcal/mol (see **Figure 10**). These results suggest a weakening of the ATP affinity when the z-z-SWCNT molecule simultaneously interacts in the same biophysical environment and considering that the obtained free energy of binding of the z-z-SWCNT molecule interacting separately with the ATP-entry-point of hVDAC1 was 70.55 kcal/mol (**Figure S1**).[12-13, 56-57] From a toxicological point of view, this fact has great significance because the MD results fit with the previous docking results and allow explaining with better clarity the binding interactions by considering the evolution of the affinity in terms of time.

Based on the individual contributions of the different components of FEB, we observed that the molecular mechanics energy (ΔE_{MM}) and non-polar solvation energy (ΔE_{apol}) increase the ATP affinity based on the negative contribution to the obtained FEB values while the polar solvation energy (ΔE_{pol}) weakens the ATP binding affinity due to its positive contribution to FEB. In terms of contributions, ΔE_{MM} potential provides a much larger contribution compared to the polar solvation energy in all the complexes, and the contribution from the non-polar solvation energy is negligibly small. Overall, the free binding energy analysis points out that the ATP molecule has a strong affinity with ATP-entry-point, which weakens in the presence of z-z-SWCNT suggesting potential channel nanotoxicity.[12-13, 56-57] (see **Figure 10**).

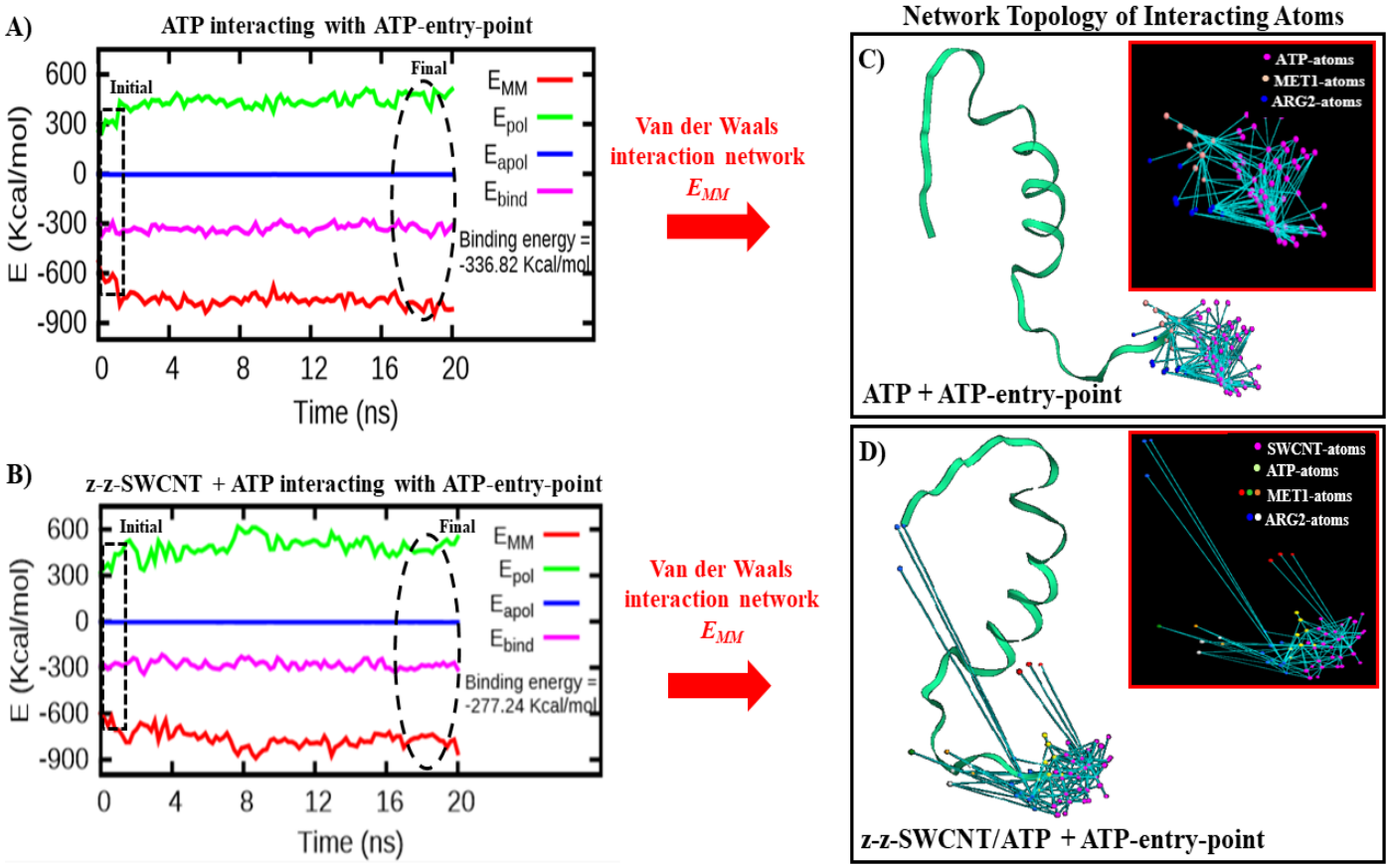

Figure 10. Representation of free binding energy (E_{bind}) decomposition for the complexes: **A)** ATP/hVDAC1 and **B)** z-z-SWCNT+ATP/hVDAC1 *vs.* simulation time (ns), highlighting the start and end of the MD simulations. The terms E_{MM}, $E_{pol} \approx G_{pol}$, $E_{apol} \approx G_{apol}$ are the average molecular mechanics potential energy (red line), polar solvation energy (green line), non-polar solvation energy (blue lines), and Gibbs binding free energy (pink line), respectively. Anisotropic network topology performed for the obtained systems based on the best energy contribution (ΔE_{MM}) to the binding free energy as **C)** ATP + ATP-entry-point and **D)** z-z-SWCNT + ATP/ATP-entry-point. Additional details can be found in the supplementary material like **Figure S1**.

The computational modeling based on the network approach for van der Waals interactions between atoms of the ligands and the ATP-entry-point reveals the existence of marked differences in the network topology when the two systems: **1)** ATP/hVDAC1 and **2)** z-z-SWCNT+ATP/ hVDAC1 (**Figure 10**; **C** and **D**) are compared. The latter analysis suggests that z-z-SWCNT near the ATP-entry-point induces conformational rearrangements of residues that can affect the physiological function of hVDAC1 in the ATP translocation.

Then, to deepen our understanding of ligand interactions with residues of the ATP-entry-point, we determined the individual contribution of the hVDAC1-residues to the binding free energy by decomposing the total binding energy. For this purpose, the decomposition energy of the complexes per residue is plotted in **Figure 11**. Inspection of **Figure 11A** suggests that the interaction between

ATP and the first five residues (like MET1, ARG2, GLY3, SER4, ALA5) of the hVDAC1 which include the ATP-entry-point activate other residue clusters starting from LEU 13 to ARG18 which are part of the surrounding area of the ATP-transport catalytic point, as mentioned above (**Figure 4E**) and also activate the VAL20 to LYS 23 in the middle of the hVDAC1 channel that favorably contributes for the stabilization of ATP molecule in the ATP-hVDAC1 complex during ATP-efflux. In the same way, **Figures 11B** and **11C** show that the interaction between z-z-SWCNT with the first five residues of hVDAC1 contributes to the increase of the binding affinity of the complexes (z-z-SWCNT/hVDAC1 and ATP + z-z-SWCNT/hVDAC1) and activates different cluster of residues from LEU 147 to LEU153 and from VAL174 to TRP 178, respectively. These results match well the molecular docking results and approach followed. It is worth pointing out that the z-z-SWCNT strongly interacts with the ATP-entry-point weakening the ATP binding affinity in ≈ - 60 kcal/mol at the ATP-entry-point and/or inactivating critical residues involved in the following steps of the ATP translocation through hVDAC1, such as the surrounding nucleotide phosphate-binding residues that cover from ASN 242 and SER 244 and the residue cluster from SER 260 to ASP 267. This response was not observed when the z-z-SWCNT is present during the interaction as depicted in **Figure 11** (**C** and **F**).

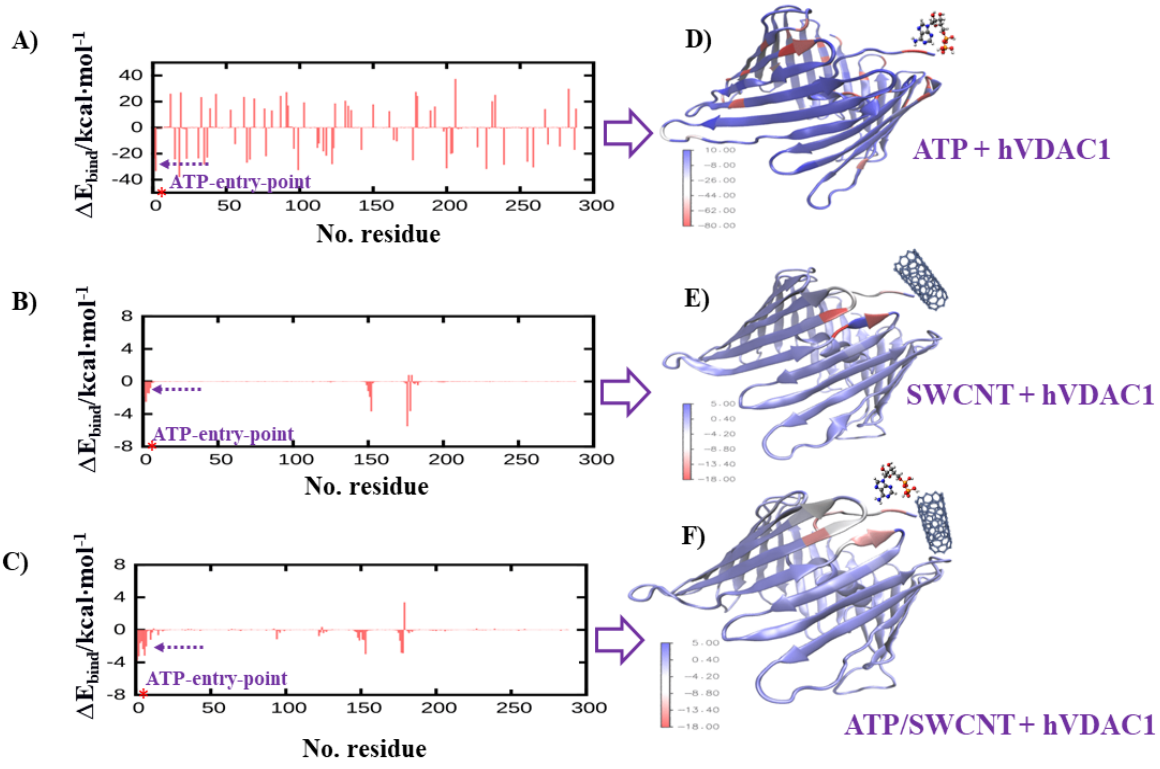

Figure 11. Left column shows a graphical representation of the binding free energy decomposition (ΔE_{bind}) per hVDAC1 residues highlighting the ATP-entry-point residues from the position of MET1 (red asterisk, *) and the corresponding binding free energy (ΔE_{bind}, like purple arrow dotted

lines) for the systems: **A)** ATP/hVDAC1, **B)** z-z-SWCNT/hVDAC1 and **C)** ATP + z-z-SWCNT/hVDAC1. Right column shows a 3D-visualization of the binding energy distribution for complexes like **D)** ATP/hVDAC1, **E)** z-z-SWCNT/hVDAC1, and **F)** ATP+ z-z-SWCNT/hVDAC1. The associated color intensity bar represents ligand interactions (ΔE_{bind}), *i.e.*: weak-interactions (blue), moderate interactions (grey) and strong interactions (red).

Lastly, all the proposed computational approaches used in the present work have been recognized and fit with the Organization for Economic Co-operation and Development (OECD) guidelines and the International Organization for Standardization on Alternative Methods in Nanotoxicology.[59,60]

No se porque pones este párrafo aquí. Quizás deberías ponerlo al final con los agradecimientos, o en la carta al editor. Pero si vosotros estáis seguros, no digo nada

Conclusions

In the present study, docking and molecular dynamics approaches were combined to study the mitochondrial channel nanotoxicity (ATP transport perturbations in hVDAC1 channel) induced by carbon nanotubes (z-z-SWCNT). The obtained results on structural and flexibility properties for ATP-entry-point (MET1, ARG2, GLY3, SER4, and ALA5) showed that these binding residues can be efficiently modeled with > 90% of conformationally-favored dihedral angles to address the study of the nanotoxicity-based interactions in the ATP-entry-point as a new and promising mitotarget. The results show that z-z-SWCNT can directly block the ATP-translocation through hVDAC1 channel from the first target-residue (MET1). Besides, the best docking pose of the evaluated z-z-SWCNT shows that the interactions with ATP-entry-point are mainly based on van der Waals hydrophobic interactions, revealing a very close relative position from the native substrate (ATP molecule).

Besides, molecular dynamics results fully match with the previous docking attainments, indicating a weakening in the binding affinity of the ATP molecule when the z-z-SWCNT molecule simultaneously interacts in the same biophysical environment (ATP-entry-point). We strongly suggest that the potential mitochondrial channel nanotoxicity (ATP transport dysfunction) of z-z-SWCNT occurs by inducing local perturbations in the inter-residue network topology and transduction properties of the ATP-entry-point. Finally, the obtained results open new opportunities towards modeling the ATP bioenergetic dysfunction induced by carbon nanomaterials, and drug discovery-based nanotechnology for precision mitochondrial nanomedicine.

Acknowledgements

The work of M. G.-Durruthy, R. Concu and M. N. D. S. Cordeiro was supported by UIDB/50006/2020 with funding from FCT/MCTES through national funds. J.M.R acknowledge Xunta de Galicia (ED41E2018/08).

Competing financial interests: The authors declare no competing financial interests.

References

1. Bayrhuber, M.; Meins, T.; Habeck, M.; Becker, S.; Giller, K.; Villinger, S.; Vonrhein, C.; Griesinger, C.; Zweckstetter, M.; Zeth, K., Structure of the human voltage-dependent anion channel. *P Natl Acad Sci USA* **2008,** *105* (40), 15370-15375.
2. Guo, X. W.; Mannella, C. A., Conformational Change in the Mitochondrial Channel, Vdac, Detected by Electron Cryomicroscopy. *Biophys J* **1993,** *64* (2), 545-549.
3. Shoshan-Barmatz, V.; Israelson, A.; Brdiczka, D.; Sheu, S. S., The voltage-dependent anion channel (VDAC): Function in intracellular signalling, cell life and cell death. *Curr Pharm Design* **2006,** *12* (18), 2249-2270.
4. Shuvo, S. R.; Ferens, F. G.; Court, D. A., The N-terminus of VDAC: Structure, mutational analysis, and a potential role in regulating barrel shape. *Bba-Biomembranes* **2016,** *1858* (6), 1350-1361.
5. Shoshan-Barmatz, V.; Zakar, M.; Rosenthal, K.; Abu-Hamad, S., Key regions of VDAC1 functioning in apoptosis induction and regulation by hexokinase. *Bba-Bioenergetics* **2009,** *1787* (5), 421-430.
6. Pi, Y. Q.; Goldenthal, M. J.; Marin-Garcia, J., Mitochondrial channelopathies in aging. *J Mol Med* **2007,** *85* (9), 937-951.
7. Zachariae, U.; Schneider, R.; Briones, R.; Gattin, Z.; Demers, J. P.; Giller, K.; Maier, E.; Zweckstetter, M.; Griesinger, C.; Becker, S.; Benz, R.; de Groot, B. L.; Lange, A., beta-Barrel Mobility Underlies Closure of the Voltage-Dependent Anion Channel. *Structure* **2012,** *20* (9), 1540-1549.
8. Ujwal, R.; Cascio, D.; Colletier, J. P.; Faham, S.; Zhang, J.; Toro, L.; Ping, P. P.; Abramson, J., The crystal structure of mouse VDAC1 at 2.3 angstrom resolution reveals mechanistic insights into metabolite gating. *P Natl Acad Sci USA* **2008,** *105* (46), 17742-17747.
9. Choudhary, O. P.; Paz, A.; Adelman, J. L.; Colletier, J. P.; Abramson, J.; Grabe, M., Structure-guided simulations illuminate the mechanism of ATP transport through VDAC1. *Nat Struct Mol Biol* **2014,** *21* (7), 626-632.
10. Okada, S. F.; O'Neal, W. K.; Huang, P. B.; Nicholas, R. A.; Ostrowski, L. E.; Craigen, W. J.; Lazarowski, E. R.; Boucher, R. C., Voltage-dependent anion channel-1 (VDAC-1) contributes to ATP release and cell volume regulation in murine cells. *J Gen Physiol* **2004,** *124* (5), 513-526.
11. Giri, A. K.; Teixeira, F.; Cordeiro, M. N. D. S., Structure and kinetics of water in highly confined conditions: A molecular dynamics simulation study. *J Mol Liq* **2018,** *268*, 625-636.
12. Gonzalez-Durruthy, M.; Werhli, A. V.; Seus, V.; Machado, K. S.; Pazos, A.; Munteanu, C. R.; Gonzalez-Diaz, H.; Monserrat, J. M., Decrypting Strong and Weak Single-Walled Carbon Nanotubes Interactions with Mitochondrial Voltage-Dependent Anion Channels Using Molecular Docking and Perturbation Theory. *Sci Rep-Uk* **2017,** *7*.
13. Gonzalez-Durruthy, M.; Werhli, A. V.; Cornetet, L.; Machado, K. S.; Gonzalez-Diaz, H.; Wasiliesky, W.; Ruas, C. P.; Gelesky, M. A.; Monserrat, J. M., Predicting the binding properties of single walled carbon nanotubes (SWCNT) with an ADP/ATP mitochondrial carrier using molecular docking, chemoinformatics, and nano-QSBR perturbation theory. *Rsc Adv* **2016,** *6* (63), 58680-58693.
14. Wang, X.; Guo, J.; Chen, T.; Nie, H. Y.; Wang, H. F.; Zang, J. J.; Cui, X. X.; Jia, G., Multi-walled carbon nanotubes induce apoptosis via mitochondrial pathway and scavenger receptor. *Toxicol in Vitro* **2012,** *26* (6), 799-806.
15. Noskov, S. Y.; Rostovtseva, T. K.; Chamberlin, A. C.; Teijido, O.; Jiang, W.; Bezrukov, S. M., Current state of theoretical and experimental studies of the voltage-dependent anion channel (VDAC). *Bba-Biomembranes* **2016,** *1858* (7), 1778-1790.

16. Forli, S.; Huey, R.; Pique, M. E.; Sanner, M. F.; Goodsell, D. S.; Olson, A. J., Computational protein-ligand docking and virtual drug screening with the AutoDock suite. *Nat Protoc* **2016,** *11* (5), 905-919.
17. Shukla, D.; Hernandez, C. X.; Weber, J. K.; Pande, V. S., Markov State Models Provide Insights into Dynamic Modulation of Protein Function. *Accounts Chem Res* **2015,** *48* (2), 414-422.
18. Briones, R.; Weichbrodt, C.; Paltrinieri, L.; Mey, I.; Villinger, S.; Giller, K.; Lange, A.; Zweckstetter, M.; Griesinger, C.; Becker, S.; Steinem, C.; de Groott, B. L., Voltage Dependence of Conformational Dynamics and Subconducting States of VDAC-1. *Biophys J* **2016,** *111* (6), 1223-1234.
19. Mitternacht, S.; Berezovsky, I. N., Coherent Conformational Degrees of Freedom as a Structural Basis for Allosteric Communication. *Plos Comput Biol* **2011,** *7* (12).
20. Keskin, O.; Durell, S. R.; Bahar, I.; Jernigan, R. L.; Covell, D. G., Relating molecular flexibility to function: A case study of tubulin. *Biophys J* **2002,** *83* (2), 663-680.
21. Greener, J. G.; Sternberg, M. J. E., AlloPred: prediction of allosteric pockets on proteins using normal mode perturbation analysis. *Bmc Bioinformatics* **2015,** *16*.
22. Oliwa, T.; Shen, Y., cNMA: a framework of encounter complex-based normal mode analysis to model conformational changes in protein interactions. *Bioinformatics* **2015,** *31* (12), 151-160.
23. Hanwell, M. D.; Curtis, D. E.; Lonie, D. C.; Vandermeersch, T.; Zurek, E.; Hutchison, G. R., Avogadro: an advanced semantic chemical editor, visualization, and analysis platform. *J Cheminformatics* **2012,** *4*.
24. Dresselhaus, G.; Riichiro, S., *Physical properties of carbon nanotubes*. World scientific: 1998.
25. Alfonsi, J.; Meneghetti, M., Small crystal approach for the electronic properties of double-wall carbon nanotubes. *New J Phys* **2009,** *11*.
26. Trott, O.; Olson, A. J., Software News and Update AutoDock Vina: Improving the Speed and Accuracy of Docking with a New Scoring Function, Efficient Optimization, and Multithreading. *J Comput Chem* **2010,** *31* (2), 455-461.
27. Lavecchia, A., Machine-learning approaches in drug discovery: methods and applications. *Drug Discov Today* **2015,** *20* (3), 318-331.
28. Smith, T. C.; Frank, E., Introducing machine learning concepts with WEKA. In *Statistical genomics*, Springer: 2016; pp 353-378.
29. Elokely, K. M.; Doerksen, R. J., Docking Challenge: Protein Sampling and Molecular Docking Performance. *Journal of Chemical Information and Modeling* **2013,** *53* (8), 1934-1945.
30. Sutherland, J. J.; Nandigam, R. K.; Erickson, J. A.; Vieth, M., Lessons in molecular recognition. 2. Assessing and improving cross-docking accuracy. *Journal of Chemical Information and Modeling* **2007,** *47* (6), 2293-2302.
31. da Silveira, C. H.; Pires, D. E. V.; Minardi, R. C.; Ribeiro, C.; Veloso, C. J. M.; Lopes, J. C. D.; Meira, W.; Neshich, G.; Ramos, C. H. I.; Habesch, R.; Santoro, M. M., Protein cutoff scanning: A comparative analysis of cutoff dependent and cutoff free methods for prospecting contacts in proteins. *Proteins* **2009,** *74* (3), 727-743.
32. Liu, K.; Kokubo, H., Exploring the Stability of Ligand Binding Modes to Proteins by Molecular Dynamics Simulations: A Cross-docking Study. *Journal of Chemical Information and Modeling* **2017,** *57* (10), 2514-2522.
33. Kitchen, D. B.; Decornez, H.; Furr, J. R.; Bajorath, J., Docking and scoring in virtual screening for drug discovery: Methods and applications. *Nat Rev Drug Discov* **2004,** *3* (11), 935-949.
34. Ballante, F.; Marshall, G. R., An Automated Strategy for Binding-Pose Selection and Docking Assessment in Structure-Based Drug Design. *Journal of Chemical Information and Modeling* **2016,** *56* (1), 54-72.
35. Hess, B.; Kutzner, C.; van der Spoel, D.; Lindahl, E., GROMACS 4: Algorithms for highly efficient, load-balanced, and scalable molecular simulation. *J Chem Theory Comput* **2008,** *4* (3), 435-447.
36. Berendsen, H. J. C.; Vanderspoel, D.; Vandrunen, R., Gromacs - a Message-Passing Parallel Molecular-Dynamics Implementation. *Comput Phys Commun* **1995,** *91* (1-3), 43-56.
37. Daura, X.; Mark, A. E.; van Gunsteren, W. F., Parametrization of aliphatic CHn united atoms of GROMOS96 force field. *J Comput Chem* **1998,** *19* (5), 535-547.
38. van Gunsteren, W. F., *Biomolecular Simulation: The GROMOS96 Manual and User Guide*. Biomos ; Zürich: 1996.
39. Berendsen, H. J. C.; Grigera, J. R.; Straatsma, T. P., The Missing Term in Effective Pair Potentials. *J Phys Chem-Us* **1987,** *91* (24), 6269-6271.
40. Giri, A. K.; Spohr, E., Conformational Equilibria of Organic Adsorbates on Nanostructures in Aqueous Solution: MD Simulations. *J Phys Chem C* **2015,** *119* (45), 25566-25575.

41. Giri, A. K.; Spohr, E., Influence of Chain Length and Branching on the Structure of Functionalized Gold Nanoparticles. *J Phys Chem C* **2018,** *122* (46), 26739-26747.
42. Giri, A. K.; Spohr, E., Cluster formation of NaCl in bulk solutions: Arithmetic vs. geometric combination rules. *J Mol Liq* **2017,** *228*, 63-70.
43. Hockney, R. W.; Eastwood, J. W., *Computer Simulation Using Particles*. CRC Press: 1988.
44. Parrinello, M.; Rahman, A., Polymorphic Transitions in Single-Crystals - a New Molecular-Dynamics Method. *J Appl Phys* **1981,** *52* (12), 7182-7190.
45. Bussi, G.; Donadio, D.; Parrinello, M., Canonical sampling through velocity rescaling. *J Chem Phys* **2007,** *126* (1).
46. Giri, A. K.; Teixeira, F.; Cordeiro, M. N. D., Salt separation from water using graphene oxide nanochannels: A molecular dynamics simulation study. *Desalination* **2019,** *460*, 1-14.
47. Essmann, U.; Perera, L.; Berkowitz, M. L.; Darden, T.; Lee, H.; Pedersen, L. G., A Smooth Particle Mesh Ewald Method. *J Chem Phys* **1995,** *103* (19), 8577-8593.
48. Darden, T.; York, D.; Pedersen, L., Particle Mesh Ewald - an N.Log(N) Method for Ewald Sums in Large Systems. *J Chem Phys* **1993,** *98* (12), 10089-10092.
49. Kumari, R.; Kumar, R.; Consortium, O. S. D. D.; Lynn, A., g_mmpbsa - A GROMACS tool for high-throughput MM-PBSA calculations. *Journal of chemical information and modeling* **2014,** *54* (7), 1951-1962.
50. Jimenez, J.; Doerr, S.; Martinez-Rosell, G.; Rose, A. S.; De Fabritiis, G., DeepSite: protein-binding site predictor using 3D-convolutional neural networks. *Bioinformatics* **2017,** *33* (19), 3036-3042.
51. Feinstein, W. P.; Brylinski, M., Calculating an optimal box size for ligand docking and virtual screening against experimental and predicted binding pockets. *J Cheminformatics* **2015,** *7*.
52. Meslamani, J.; Rognan, D.; Kellenberger, E., sc-PDB: a database for identifying variations and multiplicity of 'druggable' binding sites in proteins. *Bioinformatics* **2011,** *27* (9), 1324-1326.
53. Chen, V. B.; Arendall, W. B.; Headd, J. J.; Keedy, D. A.; Immormino, R. M.; Kapral, G. J.; Murray, L. W.; Richardson, J. S.; Richardson, D. C., MolProbity: all-atom structure validation for macromolecular crystallography. *Acta Crystallogr D* **2010,** *66*, 12-21.
54. Chennubhotla, C.; Bahar, I., Signal propagation in proteins and relation to equilibrium fluctuations. *Plos Comput Biol* **2007,** *3* (9), 1716-1726.
55. Ikeda, K.; Hirokawa, T.; Higo, J.; Tomii, K., Protein-segment universe exhibiting transitions at intermediate segment length in conformational subspaces. *Bmc Struct Biol* **2008,** *8*.
56. Park, K. H.; Chhowalla, M.; Iqbal, Z.; Sesti, F., Single-walled carbon nanotubes are a new class of ion channel blockers. *J Biol Chem* **2003,** *278* (50), 50212-50216.
57. Chhowalla, M.; Unalan, H. E.; Wang, Y. B.; Iqbal, Z.; Park, K.; Sesti, F., Irreversible blocking of ion channels using functionalized single-walled carbon nanotubes. *Nanotechnology* **2005,** *16* (12), 2982-2986.
58. Vogele, M.; Kofinger, J.; Hummer, G., Molecular dynamics simulations of carbon nanotube porins in lipid bilayers. *Faraday Discuss* **2018,** *209*, 341-358.
59. OECD Principles for the validation, for regulatory porposes of (Quantitative) Structure Activity Relationship Model, http://www.oecd.org/, accessed **13/03/2020**.
60. ISO/TC 229, *Nanotechnology*, **2011**, 1–11, Draft 4.